Journal of Power Sources, 35 (1991) 131–142

Passivation of iron in alkaline carbonate solutions

M. Jayalakshmi and **V. S. Muralidharan***
Central Electrochemical Research Institute, Karaikudi 623006, Tamilnadu (India)

(Received November 18, 1990)

Abstract

Carbonation affects the performance of alkaline secondary batteries employing strongly alkaline solutions. In Ni/Fe cells, carbonate has a deleterious effect on the iron electrode. In 6 M KOH, $FeCO_3$ is formed by a dissolution–precipitation mechanism. The oxidation of divalent iron to trivalent iron involves the diffusion of OH^-. Carbonates prevent both this diffusion and the oxidation by forming a salt film on the surface. In excess carbonate, soluble iron carbonate complexes are formed. During the reduction process, $FeCO_3$ is formed by the reductive dissolution of FeOOH; carbonate hinders the reduction of divalent iron to iron.

Introduction

Understanding the passivation of iron in alkaline carbonate solutions is particularly important in connection with the use of iron as a rechargeable anode in electrochemical cells. In aqueous HCO_3^- and CO_3^{2-} solutions, galvanostatic polarization plots exhibit two arrests [1, 2] that are attributed to: (i) the formation of a film consisting of ferrous carbonate and hydroxides; (ii) the oxidation of the film to ferric oxide. Potentiostatic and dynamic [3–7] studies reveal two oxidation peaks; the former is due to the formation of an oxide of iron and ferrous carbonate, and the latter to γ-ferric oxide or Fe_3O_4. In HCO_3^-/CO_3^{2-} buffer solutions, the early passivation of iron is due to oxides/hydroxides, and carbonates do not participate in the reaction. This paper reports an attempt to identify the oxidation/reduction of divalent/trivalent iron and the passivation of iron in the potential range -400 to -700 mV in 6 M KOH solutions containing carbonate species.

Experimental

Cyclic voltammetric and chronocoulometric experiments were conducted on an iron electrode of 99.9999% purity (Johnson-Matthey, U.S.A.) and 0.2 cm^2 in area. A platinum counter electrode and an Hg/HgO reference electrode were used. All potentials are reported with regard to the latter electrode.

*Author to whom correspondence should be addressed.

0378-7753/91/$3.50

Solutions of 6 M KOH containing various carbonate concentrations ($0.1 > x > 1.0$ M) were prepared from AnalaR chemicals and double-distilled water.

Cyclic voltammetric experiments were carried out between switching potentials of -1.3 and 0.9 V. A double potential step chronocoulogram was also performed. From an initial potential of -400 mV, the electrode was stepped down to -700 mV and the accompanying charge was measured as a function of time. The potential was then stepped back to -400 mV after a pulse width of 250 ms. The resulting charge was again monitored.

Results

Cyclic voltammetry

Figure 1 shows the cyclic voltammograms obtained for iron in both the presence and the absence of carbonate in 6 M KOH solution. In the absence of carbonate, two anodic peaks and two cathodic peaks are observed; these features have been investigated in detail [8, 9]. The voltammetric characteristics are unaffected by the presence of carbonate, except that the third cathodic peak appears as a limiting plateau and the fourth peak becomes much more prominent.

Increase in carbonate concentration results in a shift of $E_{p,a}$(II) to a more negative value and $E_{p,c}$(III) and $E_{p,c}$(IV) to more positive values. It is noticeable that, with the exception of peak(IV), the charges under the anodic and cathodic peaks are considerably reduced.

At higher scan rates ($100 > v < 1000$ mV s^{-1}), the cyclic voltammograms obtained in the presence of carbonate exhibit an additional limiting plateau

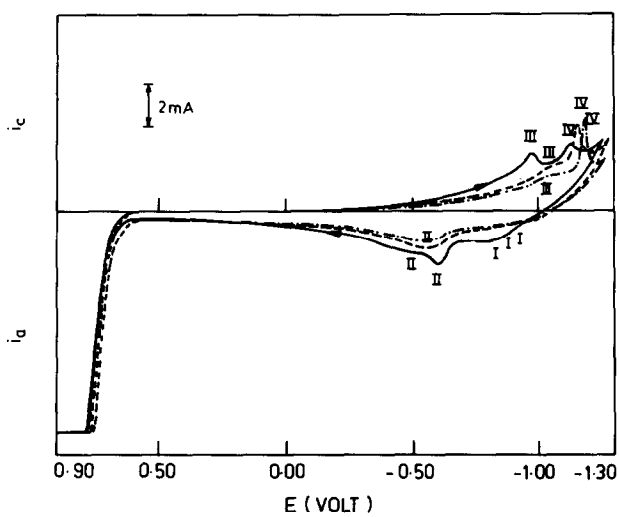

Fig. 1. Cyclic voltammograms for iron in: ——, 6 M KOH; – – –, 6 M KOH + 0.1 M Na_2CO_3; – . –, 6 M KOH + 1 M Na_2CO_3. Scan rate 75 mV s^{-1}.

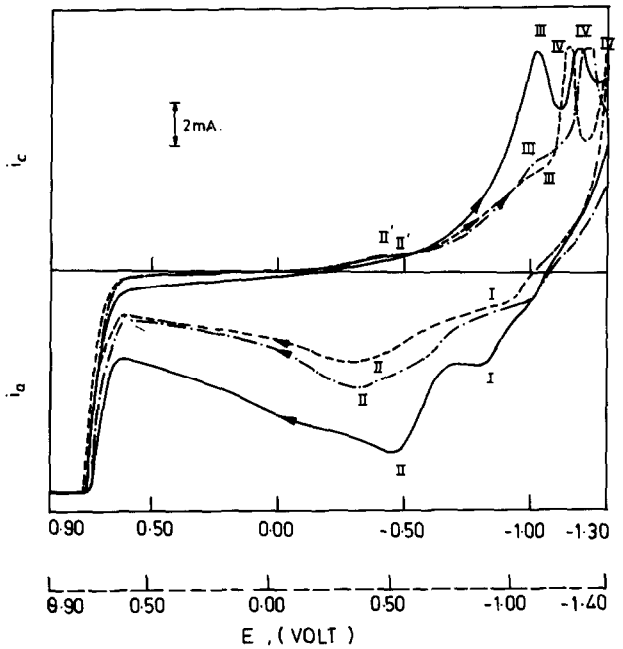

Fig. 2. Cyclic voltammograms for iron in: ——, 6 M KOH; – – –, 6 M KOH + 0.1 M Na_2CO_3; – . –, 6 M KOH + 1 M Na_2CO_3. Scan rate 500 mV s^{-1}.

around −500 mV in the negative-going scan (Fig. 2). In order to discover the reaction occurring in this potential range, chronocoulometric studies were made over the potential range −400 to −700 mV.

Chronocoulometry

The forward and backward (−400 to −700 mV) chronocoulometric responses (Fig. 3) for the oxidation of divalent iron to trivalent iron indicate a time-dependent variation of the total charge, Q. As the charges associated with the electrical double-layer and the adsorbed species are time-independent, the variation of Q with t may also involve a component due to diffusion, most probably the diffusion of OH^- ions in the passive film.

Discussion

The oxidation and reduction processes occurring on iron during voltammetry have recently been reviewed [10]. X-ray, electron diffraction, and electrochemical methods have identified the anodic films formed, under varying conditions and potentials, as $Fe(OH)_2$, Fe_3O_4, Fe_2O_3 or γ-$Fe_2O_3 \cdot H_2O$.

Positive-going scan

Behaviour in −1000 to −700 mV region

During the positive-going scan, the initial portion of the curve before the appearance of the second peak is due to the oxidation of adsorbed

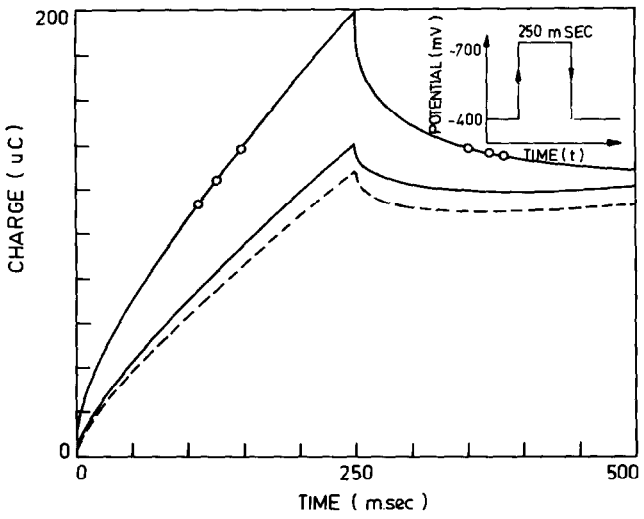

Fig. 3. Chromocoulograms for iron in: ——, 6 M KOH; – – –, 6 M KOH + 0.1 M Na_2CO_3; – . –, 6 M KOH + 1.0 M Na_2CO_3.

hydrogen [11], or iron [12], or both [12]. With iron powder, it was observed earlier [13] that the oxidation of adsorbed hydrogen occurred only at −1000 mV and, hence, it was claimed that the initial portion of the curve is due to $Fe \rightarrow FeOH_{ads}$. The latter is oxidised to $Fe(OH)_2$ as follows:

$$Fe + OH^- \rightleftharpoons FeOH_{ads} + e^- \quad (1)$$

$$FeOH_{ads} \longrightarrow FeOH_{ads}^+ + e^- \quad (2)$$

$$Fe(OH)_{ads}^+ + OH^- \rightleftharpoons Fe(OH)_2 \quad (3)$$

The thermodynamics of the $Fe-CO_2-H_2O$ system shows that ferrous carbonate is a stable phase. The formation of $FeCO_3$ can occur via:

$$Fe(OH)_2 + CO_3^{2-} \longrightarrow FeCO_3 + 2OH^- \quad (4)$$

The growth of oxide can take place through the electrodissolution of iron via hydrated $Fe(OH)_2$ [14]. For the pH range 8.7–10.7, it was suggested that $FeCO_3$ is the first solid phase and that carbonates act as a catalyst in the dissolution reaction. The presence of both $FeCO_3$ and $Fe(OH)_2$ at pH 11.8 was confirmed by X-ray diffraction studies. In 6 M KOH solutions, however, $FeCO_3$ may also be formed by:

$$HFeO_2^- + CO_3^{2-} + H_2O \longrightarrow FeCO_3 + 3OH^- \quad (5)$$

Soluble Fe(II) and Fe(III) species had been detected earlier [15].

Second anodic peak

The divalent hydroxides and carbonates have low porosity and hinder the diffusion of OH^- ions necessary for their growth. The second oxidation step of the iron electrode involves the formation of δ-FeOOH during the first cycle.

$$Fe(OH)_2 + OH^- \longrightarrow \delta\text{-}FeOOH + H_2O + e^- \quad (6)$$

On further cycling, magnetite formation is favoured [16]:

$$3Fe(OH)_2 + 2OH^- \rightleftharpoons Fe_3O_4 \cdot 4H_2O + 2e^- \quad (7)$$

In the absence of carbonate, the oxidation of iron in 6 M KOH solutions is as shown in eqn. (6). The reaction product, FeOOH, can dissolve to yield an Fe(III) species, i.e.,

$$FeOOH + OH^- \rightleftharpoons FeO_2^- + H_2O \quad (8)$$

$$HFeO_2^- + 2FeO_2^- + H_2O \rightleftharpoons Fe_3O_4 + 3OH^- \quad (9)$$

In alkaline carbonate solutions, the passive film can grow at certain points and extend over the surface as a layer of uniform thickness, δ [17]. The carbonates so formed present an ohmic resistance to the flow of current, as witnessed by the decrease in peak currents in presence of carbonates at all sweep rates (Fig. 1). If A is the total area of the electrode and Q_p is the degree of coverage on the electrode, then the resistance of the solution in the pores of the passive layer, R_p, is given by [18]:

$$R_p = \{\delta/KA(1-\theta_p)\} \quad (10)$$

The expressions for the current and the potential at the peak are:

$$E_{p,a} = E_0 + \sqrt{\frac{nF\rho K}{M}}\{(\delta/k) + R_o A(1-\theta_p)\}\sqrt{v} \quad (11)$$

$$i_{p,a} = \left(\frac{\sqrt{nF\rho K}}{M}\right)A(1-\theta_p)\sqrt{v} \quad (12)$$

As predicted by these equations, the second anodic peak current disappears as $v \to 0$ (Fig. 4). The $E_{p,a}$(II) values are extrapolated to $v \to 0$ to obtain E_0 (Fig. 5). The latter is the minimum potential for the formation of δ-FeOOH. Increase of carbonate shifts these potentials to more noble values. This suggests that carbonate prevents the oxidation of divalent iron. An estimate of θ_p after the second peak can be obtained by assuming: $\rho_{FeOOH} = 5.2$ g cm^{-3}; $M = 88.85$ g mol^{-1}; $K = 10^{-2}$ ohm^{-1} cm^{-1}. The value of $\{\{E_{p,a}(II) - E_0\}/i_{p,a}(II)\}$ has the dimensions of resistance. It was found that θ_p values increased from 0.92 to 0.95 in carbonate solutions (Table 1). The increased surface coverage prevents the diffusion of OH^- ions into the metal and thus hinders the latter's further oxidation.

Beyond -400 mV, the decrease in current (Fig. 1) is due to the complete coverage of the surface by trivalent oxides. This is confirmed by the near capacitative behaviour observed before oxygen evolution.

Negative-going scan

From the theory of electrochemical formation of metallic oxides using a chronoamperometric method with linear variation of potential [19], the

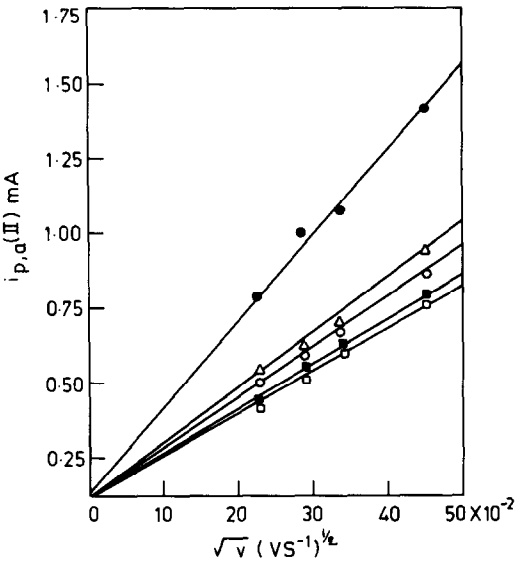

Fig. 4. $i_{p,a}$(II) vs. $\sqrt{v}$ for iron in: ●, 6 M KOH; △, 6 M KOH + 0.1 M Na_2CO_3; ○, 6 M KOH + 0.2 M Na_2CO_3; ■, 6 M KOH + 0.3 M Na_2CO_3; □, 6 M KOH + 0.5 M Na_2CO_3.

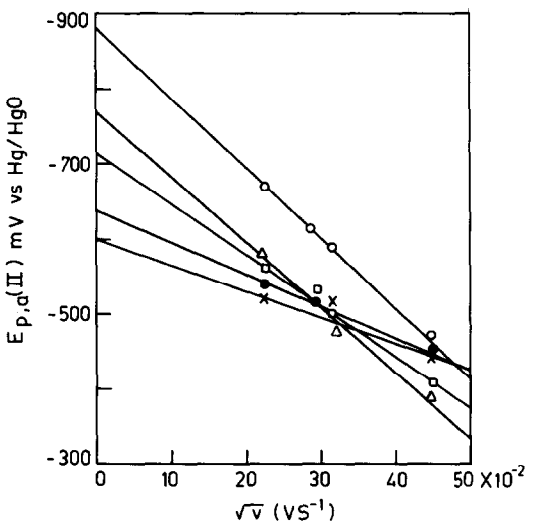

Fig. 5. $E_{p,a}$(II) vs. $\sqrt{v}$ for iron in: ○, 6 M KOH; △, 6 M KOH + 0.2 M Na_2CO_3; □, 6 M KOH + 0.3 M Na_2CO_3; ●, 6 M KOH + 0.5 M Na_2CO_3; ×, 6 M KOH + 1 M Na_2CO_3.

appearance of a limiting current, or plateau, in the E–i curves suggest a situation where one or more oxides are soluble and the formation of the oxides obeys the Langmuir and Temkin–Frumkin conditions. During the negative-going scan, a plateau or limiting-current (Fig. 6) region is observed. This transforms to a peak at high scan rates. The dependence of this on log v and the fact that [d log $i_{p,c}$(III)/d log v] CO_3^{2-}, $OH^- = 0.5$ suggest

TABLE 1

Parameters derived from eqns. (11) and (12)

Solution	E_0 (mV)	θ_p
6 M KOH	–	0.917
6 M KOH + 0.1 M Na_2CO_3	−825	0.954
6 M KOH + 0.2 M Na_2CO_3	−750	0.954
6 M KOH + 0.3 M Na_2CO_3	−715	0.954
6 M KOH + 0.5 M Na_2CO_3	−650	0.954
6 M KOH + 1 M Na_2CO_3	−590	0.954

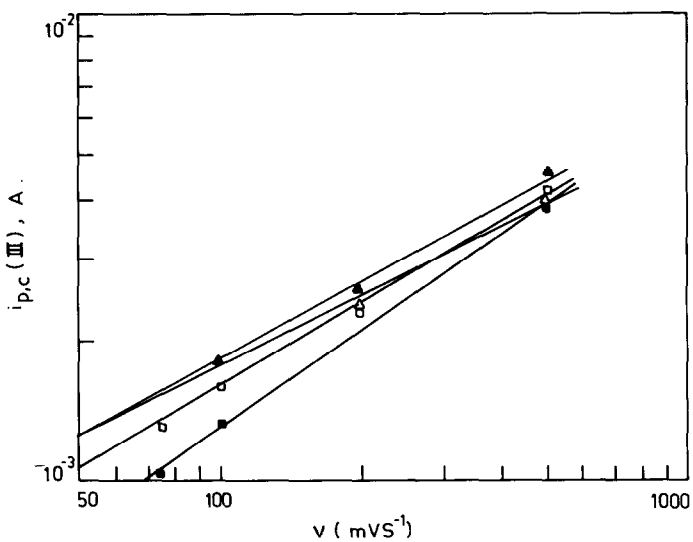

Fig. 6. $i_{p,c}$(III) vs. log v for iron in: ▲, 6 M KOH + 0.1 M Na_2CO_3; △, 6 M KOH + 0.2 M Na_2CO_3; □, 6 M KOH + 0.3 M Na_2CO_3; ■, 6 M KOH + 0.5 M Na_2CO_3.

charge transfer coupled with chemical reaction. Further, $Q_c(III) > A_a(I)$ indicates a reductive dissolution of oxides coupled with chemical reaction.

The appearance of cathodic peak (IV) with a potential that becomes more active with carbonate shows that the reduction of divalent iron is difficult and that $[\mathrm{d} \log i_{p,c}(IV)/\mathrm{d} \log {CO_3}^{2-}]_{OH^-,v} = 0.25$. The increase in the cathodic peak current (IV) with carbonate suggests that $FeCO_3$ is also reduced, along with $Fe(OH)_2$, to iron.

In order to understand the oxidation/reduction behaviour in the −400 to −700 mV potential region, double potential step (chronocoulograms) experiments were performed. It was found (see above) that Q varied with t. Furthermore, plots of Q versus $t^{1/2}$ are linear (i.e., Anson plots) (Fig. 7). This suggests that the diffusion is slow. The diffusing species are OH^- ions that move towards the solution during the forward step (0–250 ms).

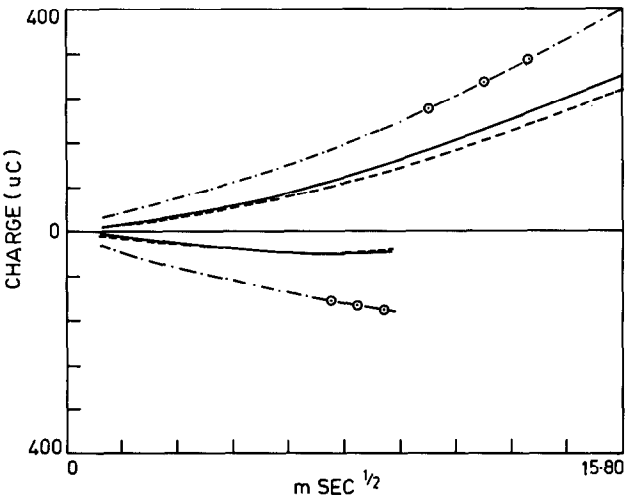

Fig. 7. Q vs. $\sqrt{t}$ for iron in: ——, 6 M KOH; – – –, 6 M KOH + 0.1 M Na_2CO_3; – . –, 6 M KOH + 1 M Na_2CO_3.

It is possible to calculate the surface excess of OH^- ions in both the forward and backward steps: The forward chronocoulometric response can be described by [20]:

$$Q = Q_d + Q_{dl} + nFA\Gamma_{OH^-} \tag{13}$$

where

$$Q_d = \left[\frac{2nFA\sqrt{D}}{\sqrt{\pi}}\right] C_{OH^-};$$

Q_{dl} = capacitative charge (C);
Γ_{OH^-} = surface excess (mol cm^{-2});
D = diffusion coefficient (10^{-5} cm^2 s^{-1});
C_{OH^-} = concentration of OH^- ions in the film.
When the step is reversed after 250 ms, the oxidation proceeds and

$$Q_r\ (t > \tau) = Q_{dl} + \left\{\frac{2nFA\sqrt{DC_{OH^-}}}{\sqrt{\Lambda}}\right\} \theta \tag{14}$$

where:
$Q = \{\sqrt{t} - (t-\tau)^{1/2} - t^{1/2}\}$;
τ = forward step width (s);
t = total integration time (s).
$Q(t > \tau)$ was found to vary linearly with θ (Fig. 8) and Q_{dl} was evaluated. Using the Q_{dl} values, the surface excess of OH^- ions was evaluated from the intercept of the Anson plots. The variation of C_{OH^-} with carbonate can also be understood from the corresponding slope values (Tables 2, 3).

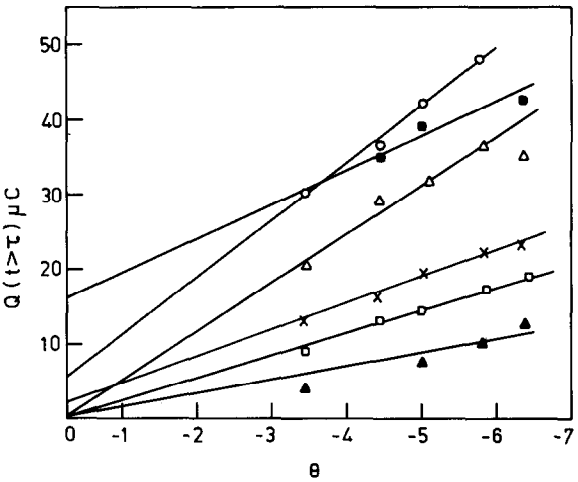

Fig. 8. Q $(t>\tau)$ vs. θ plot for iron in: ○, 6 M KOH; ×, 6 M KOH+0.1 M Na_2CO_3; △, 6 M KOH+0.2 M Na_2CO_3; ■, 6 M KOH+0.3 M Na_2CO_3; □, 6 M KOH+0.5 M Na_2CO_3; ▲, 6 M KOH+1.0 M Na_2CO_3.

TABLE 2

Parameters derived from chronocoulograms in the forward step (−400 to −700 mV)

Solution	Slope Q_d (μC ms$^{-1/2}$)	Q_{dl} (μC)	Γ_{OH^-} (mol cm^{-2}) $\times 10^{-2}$
6 M KOH	22.9	5	−437.5
6 M KOH+0.1 M Na_2CO_3	20.9	3	−411.5
6 M KOH+0.2 M Na_2CO_3	18.5	1	−322.9
6 M KOH+0.3 M Na_2CO_3	15.4	0.5	−346.4
6 M KOH+0.5 M Na_2CO_3	16.5	2.5	−335.9
6 M KOH+1 M Na_2CO_3	15.1	1.6	−145.8

TABLE 3

Parameters derived from chronocoulograms in the backward step (−400 to −700 mV)

Solution	Slope Q_d (μC ms$^{-1/2}$)	Q_{dl} (μC)	Γ_{OH^-} (mol cm^{-2}) $\times 10^{-2}$
6 M KOH	0.0	5	183.4
6 M KOH+0.1 M Na_2CO_3	–	3	–
6 M KOH+0.2 M Na_2CO_3	4.7	1	98.4
6 M KOH+0.3 M Na_2CO_3	–	0.5	–
6 M KOH+0.5 M Na_2CO_3	1.6	2.5	98.5
6 M KOH+1 M Na_2CO_3	5.5	16	29.1

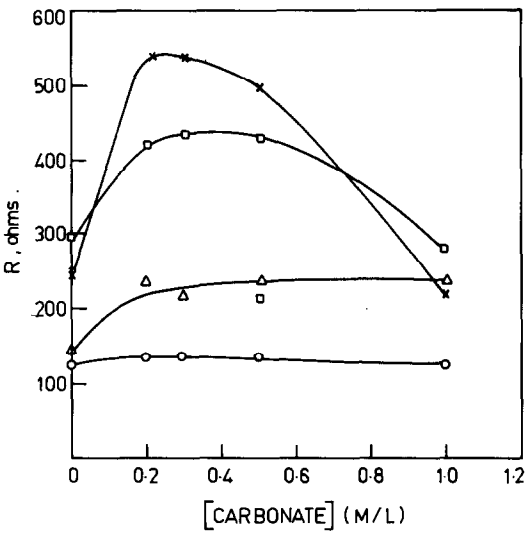

Fig. 9. R vs. [Carbonate] concentration at different scan rates: ×, 75; □, 100; △, 200; ○, 500 mV s^{-1}.

Tables 2 and 3 show that Γ_{OH^-} decreases in both the forward (reduction) and backward (oxidation) steps in the presence of carbonates. In 6 M KOH, Γ_{OH^-} is greater in the reduction process. This is understandable as OH^- ions are released during reduction and consumed during oxidation. In alkaline carbonate solutions, a competitive adsorption between OH^- ions and carbonate ions takes place and an increase of CO_3^{2-} in solution decreases the surface excess of hydroxide ions, Γ_{OH^-}. On anodic polarisation, adsorbed carbonates can diffuse inside the oxide and the carbonate content may decrease the OH^- ion concentration inside the oxide film. The diffusion of CO_3^{2-} ion inside the oxide lattice depends on the field and the concentration of CO_3^{2-} ions that is adsorbed. With time, the latter may increase in the film and the surface become covered with carbonates. The $FeCO_3$ formed may also dissolve in excess carbonate (desorption of carbonate) to form soluble $[Fe(CO_3)_2]^{2-}$, i.e.,

$$FeCO_3 + {CO_3^{2-}}_{ads} \longrightarrow [Fe(CO_3)_2]^{2-}_{solution} \tag{15}$$

At high scan rates with increased anodic polarisation:

$$[Fe(CO_3)_2]^{2-} \longrightarrow [Fe(CO_3)_2]^- + e^- \tag{16}$$

There is competition between the two processes: carbonate ion desorption and its diffusion in solution, and adsorption and diffusion in the passive film.

At higher scan rates, desorption of carbonate takes place. Conversely, diffusion inside the film is favoured at lower rates. As the scan rate decreases, the resistance of the film (R) increases (Fig. 9). At 75 mV s^{-1}, the maximum resistance (R value) was observed with 0.2 M Na_2CO_3. The subsequent

decrease in resistance with carbonate suggests that desorption is predominant with increasing carbonate concentration. As $v \rightarrow 0$, both the resistance and the θ_p values reach a maximum. It would appear, therefore, that the oxide becomes saturated with carbonates and the surface becomes covered with CO_3^{2-} ions. Further oxidation results in the conversion to FeOOH:

$$Fe(CO_3) + 3OH^- \longrightarrow FeOOH + CO_3^{2-} + H_2O \quad (17)$$

During the reduction process, the C_{OH^-} in the film is comparable with that in the oxidation process. The outward diffusion of OH^- ions is hindered during reduction, perhaps by the protective nature of the passive film or the precipitate formed on the surface.

The appearance of a cathodic plateau (II') in carbonate solutions alone (Fig. 2) suggests that:

$$[(Fe(CO_3)_2]^- + e^- \longrightarrow [Fe(CO_3)_2]^{2-}_{solution} \quad (18)$$

Trivalent oxide reduction can occur as:

$$FeOOH + H_2O \rightleftharpoons HFeO_2^- + H_2O + e^- \quad (19)$$

and

$$HFeO_2^- + CO_3^{2-} \longrightarrow FeCO_3 + 3OH^- \quad (20)$$

Reaction (20) causes an increase in Γ_{OH^-} during reduction.

The surface at -1000 mV has $FeCO_3$ formed by reduction. This offers higher overvoltages for divalent iron reduction and enhancement of the cathodic peak current (IV) is due to reduction of both $FeCO_3$ and $Fe(OH)_2$ to iron.

Conclusions

In carbonate-containing 6 M KOH solutions, $FeCO_3$ is formed by a dissolution–precipitation mechanism. The oxidation of divalent iron to trivalent oxides involves the diffusion of OH^- ions. Carbonates prevent this diffusion and oxidation by forming a salt film on the surface. In excess carbonate, soluble iron carbonate complexes are formed. During the reduction process, $FeCO_3$ is formed by the reductive dissolution of FeOOH. Carbonates prevent the reduction of divalent iron to iron.

List of symbols

$E_{p,a}$	Anodic peak potential (mV)
$i_{p,a}$	Anodic peak current (A)
E_0	Film formation potential (mV)
R_p	Resistance of solution in pores (Ω)
ρ	Film density

δ	Thickness of film (cm)
K	Specific conductivity of solution inside pores (Ω^{-1} cm^{-1})
θ_p	Degree of coverage of electrode (cm)
A	Area of electrode (cm^2)
$E_{p,c}$	Cathodic peak potential (mV)
$i_{p,c}$	Cathodic peak current (A)
D_{OH^-}	Diffusion coefficient of OH^- ion (cm^2 s^{-1})
v	Scan rate, (mV s^{-1})
C_{OH^-}	Concentration of OH^- ion
R_o	Resistance of solution external to film
M	Molecular weight of FeOOH
R	Resistance of passive film
Q	Total chronocoulometric charge (C)
Q_d	Charge due to diffusion (C)
Q_{dl}	Capacitative charge (double layer) (C)
Γ_{OH^-}	Surface excess of OH^- ion (mol cm^{-2})
t	Total integration time (s)
τ	Forward step width (s)
n	No. of electrons
F	Faraday (C)

References

1 P. Hancock and J. E. O. Mayne, *J. Appl. Chem. (London)*, *9* (1959) 345.
2 D. Gilroy and J. E. O. Mayne, *Br. Corros. J.*, *1* (1966) 161.
3 F. Clerbois and J. Massart, *Corros. Sci.*, *2* (1962) 1.
4 J. G. N. Thomas, T. J. Nurse and R. Walker, *Br. Corros. J.*, *5* (1970) 87.
5 J. A. Von Fraunhofer, *Corros. Sci.*, *10* (1970) 245.
6 R. D. Armstrong and A. C. Coates, *J. Electroanal. Chem.*, *50* (1974) 303.
7 J. M. Sutcliffe, R. R. Fessler, W. K. Boyd and R. N. Parkins, *Corrosion*, *28* (1983) 1627.
8 V. S. Muralidharan and M. Veerashanmugamani, *J. Appl. Electrochem.*, *15* (1985) 675.
9 G. Paruthimal Kalaignan, V. S. Muralidharan and K. I. Vasu, *J. Appl. Electrochem.*, *17* (1987) 1083.
10 J. Cerny and K. Micka, *J. Power Sources*, *25* (1989) 111.
11 D. Geana, A. A. El Miligy and W. J. Lorenz, *J. Appl. Electrochem.*, *4* (1974) 337.
12 L. D. Burke and M. E. G. Lyons, *J. Electroanal. Chem.*, *198* (1986) 347.
13 H. Cnobloch, D. Gröppel. W. Nippe and F. V. Sturm, *Chem. Ing. Tech.*, *45* (1973) 203.
14 C. M. Rangel, R. A. Leitao and I. T. Fonseca, *Electrochim. Acta*, *31* (1986) 1659.
15 R. D. Armstrong and T. Baurhoo, *J. Electroanal. Chem.*, *34* (1972) 41; *40* (1972) 325.
16 T. K. Teplinskaya, N. N. Fedorova and S. A. Rozentsveig, *Zh. Fiz. Khim.*, *38* (1964) 2176.
17 W. J. Muller, *Trans. Faraday Soc.*, *27* (1931) 737.
18 V. S. Muralidharan, K. Thangavel and K. S. Rajagopalan, *Electrochim. Acta*, *28* (1983) 1611.
19 A. M. Baticle, R. P. Veerareau and J. Vernieres, *J. Electroanal. Chem.*, *45* (1973) 439.
20 A. J. Bard and L. R. Faulkner, *Electrochemical Methods – Fundamentals and Applications*, Wiley, NY, 1980, p. 199.